Assessing cardiac stiffness using ultrasound shear wave elastography

Annette Caenen[a,b,c], Mathieu Pernot[d], Kathryn R. Nightingale[e], Jens-Uwe Voigt[b,f], Hendrik J. Vos[c], Patrick Segers[a*], Jan D'hooge[b*]

[a]*IbiTech-bioMMeda, Ghent University, Ghent, Belgium.*

[b]*Department of Cardiovascular Sciences, University of Leuven, KU Leuven, Leuven, Belgium.*

[c]*Department of Cardiology, Erasmus MC University Medical Center, Rotterdam, the Netherlands.*

[d]*Physics for Medicine, INSERM, CNRS, ESPCI, PSL University, Paris, France.*

[e]*Department of Biomedical Engineering, Duke University, Durham (NC), United States.*

[f]*Department of Cardiovascular Diseases, University Hospital Leuven, KU Leuven, Leuven, Belgium.*

**Joint last author.*

Address for correspondence:

Annette Caenen, IBiTech-bioMMeda, Ghent University, Campus Heymans - Blok B, Corneel Heymanslaan 10, 9000 Gent, Belgium. Phone: +32 9 332 02 58. Email: annette.caenen@ugent.be

Abstract

Shear wave elastography offers a new dimension to echocardiography: it measures myocardial stiffness. Therefore, it could provide additional insights into the pathophysiology of cardiac diseases affecting myocardial stiffness and potentially improve diagnosis or guide patient treatment. The technique detects fast mechanical waves on the heart wall with high frame rate echography, and converts their propagation velocity into a stiffness value. A proper interpretation of shear wave data is required as the shear wave interacts with the intrinsic, yet dynamically changing geometrical and material characteristics of the heart under pressure. This dramatically alters the wave physics of the propagating wave, demanding adapted processing methods compared to other shear wave elastography applications as breast tumor and liver stiffness staging. Furthermore, several advanced analysis methods have been proposed to extract supplementary material features such as viscosity and anisotropy, potentially offering additional diagnostic value. This review explains the general mechanical concepts underlying cardiac shear wave elastography and provides an overview of the preclinical and clinical studies within the field. We also identify the mechanical and technical challenges ahead to make shear wave elastography a valuable tool for clinical practice.

Introduction

Echocardiographic evaluation of cardiac function is indispensable for the diagnosis and treatment of any cardiovascular disease. For many years, various indices based on measures of ventricular geometry and/or velocity measurements of blood flow and tissue have been proposed for the assessment of systolic or diastolic function, but none of these allow for a complete description of cardiac function. Indeed, cardiac distensibility and contractility – two important determinants of cardiac function – are tightly intertwined with active and passive myocardial stiffness, which is intrinsically linked with alterations at the level of the cardiomyocytes, crossbridge actin-myosin interactions and the composition of the extracellular matrix. Non-invasive ultrasound based evaluation of tissue stiffness started in the late 1980s to early 1990s, when a field based on the old technique of palpation was founded: ultrasound (US) elastography (1,2). Later, around 2010, the advent of high-frame rate imaging meant a dogma shift for medical US: the entire field of view was insonified for every transmit in order to enable image reconstruction on receive at high frame rates (> 500 frames/s) in contrast to the conventional line-by-line scanning. This high frame rate imaging modality enabled new methodologies in elastography (3). In this review, we focus on one specific class of high frame rate techniques, referred to as shear wave elastography (SWE).

SWE – as the name suggests – uses the propagation characteristics of shear waves to estimate the stiffness of the tissue in which they propagate. Shear waves are naturally induced in the heart upon closure of atrio-ventricular or ventriculo-arterial valves, but may also be mechanically induced using an external source. SWE has been clinically successful in various non-cardiac domains, such as staging liver fibrosis (4) and characterizing malignant breast lesions (5). The potential of the method to directly assess passive – and active – myocardial stiffness exists, but the method is faced with challenges relating to its fundamental working principles when applied to the heart. Indeed, the geometrical and mechanical properties of the heart – thin-walled, anisotropic, layered, actively contracting (in short: *mechanical factors*) – are more complex than that of large nonlinear viscoelastic organs such as the breast and the liver, evoking an altered wave physics that obeys different physical principles. With it, also the interpretation of the observed shear waves and the deduction of tissue properties becomes more complex.

This paper reviews the basic concepts of cardiac ultrasound SWE and gives an overview of the (pre)clinical studies that have investigated the effect of one or multiple mechanical factors and pathology on shear wave propagation. This way, the reader will be able to better understand shear wave measurements in the cardiac setting and interpret findings from a biophysical point of view. Shear wave speed values reported for healthy volunteers and various preclinical and patient studies (myocardial infarction, hypertrophic cardiomyopathy, amyloidosis, heart transplantation, hypertension) are summarized. The paper concludes with recommendations on uniform reporting and identification of the main mechanical (and technical) challenges ahead.

Definitions

The *stiffness* of a solid material, such as cardiac tissue, relates to the relation between its loading and subsequent deformation, typically described by the normalized physical quantities *stress* and *strain respectively*. In continuum mechanics, one typically expresses *material stiffness (*or

modulus) as the mathematical relationship between stress and strain. In clinical practice (where it is often impossible to assess stress and strain), one often uses *structural stiffness*, which depends on material stiffness but also on its geometry and boundary conditions (6,7). Biological tissue is often approximated as a *linear elastic isotropic* material in the field of elasticity imaging, in which the stress σ linearly depends on the strain ε regardless of the material's orientation (i.e. isotropy), as visualized in Figure 1a. The slope of the curve represents the *elasticity* or *Young's modulus E*, expressing the material's resistance to uniaxial tension/compression. The relative material deformation in the direction perpendicular to the loading direction is then given by *Poisson's ratio* υ. Other important moduli that describe the material's response to different kinds of loading are the *shear modulus* μ (material's resistance to simple shear loading) and the *bulk modulus* K (material's resistance to volumetric changes).

The linear elastic isotropic material model is a good first order approximation for some tissues (e.g. liver), but in general material properties of tissue are essentially dependent on material orientation (*anisotropy*), time *(viscoelasticity)* and stretch state (*material non-linearity* or *hyperelasticity)*, as shown in Figure 1. This figure also demonstrates the meaning of *instantaneous* or *operational* stiffness (local slope of the (ε,σ)-relationship): a higher instantaneous stiffness – indicated by E_{high} in Figure 1b – might be related to higher strains (hyperelastic effect), higher strain rate (viscoelastic effect) or fiber orientation (anisotropic effect). In addition, the apparent stiffness of a muscle can be modified by internal stress induced by active contraction.

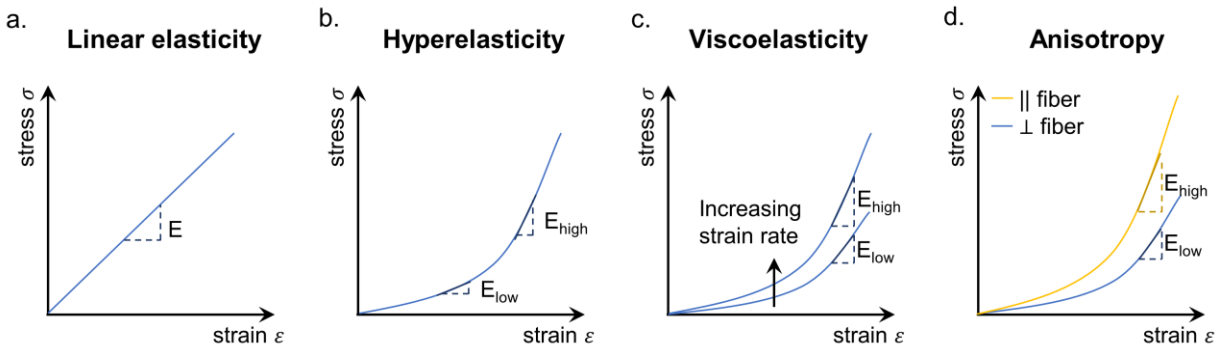

Figure 1 – Mechanical engineering definitions: conceptual representation of linear elasticity (a), hyperelasticity (b), viscoelasticity (c) and anisotropy (d) in terms of stress-strain curves.

Theoretical background – relating stiffness to wave propagation

Theoretically, only two wave modes can exist in an isotropic bulk material: a *shear* wave, and a *compressional* wave. These wave modes are distinct in the local particle motion (or deformation) relative to the direction of propagation (see Figure 2a): a shear or transversal wave has particle motion perpendicular to the propagation direction, whereas a compressional (or longitudinal) wave particle motion parallel to the propagation direction. These compressional waves are the acoustic waves that are used for standard echography. The propagation speeds of these two wave types are linked to different tissue material properties of the medium in which they

propagate. When approximating tissue as an *infinite isotropic linear elastic medium*, the following relations hold true (8):

$$c_T = \sqrt{\frac{\mu}{\rho}} \quad (1)$$

$$c_L = \sqrt{\frac{K + \frac{4}{3}\mu}{\rho}} \quad (2)$$

with shear wave propagation speed c_T, shear modulus μ, mass density ρ, longitudinal wave propagation speed c_L, and bulk modulus K.

It is important to stress that pure shear and compression waves only exist in an infinite, homogenous, isotropic medium, for which Eqs. 1 and 2 describe the wave propagation velocities. When the geometry becomes confined, or when material properties are inhomogeneous or direction-dependent – all of which are true for the myocardium – other wave modes than a shear wave might be present or be generated (e.g. vertical/horizontal shear waves in transverse isotropic media (9,10), Lamb waves in plate-like geometries (11,12)). Wave motion can then have a longitudinal component next to a transversal component. This should be considered when interpreting the mechanical waves detected with echocardiography and will be discussed in detail further in this review (see *Shear wave imaging and reconstruction of shear wave speed maps).*

In principle, both shear and bulk modulus are expected to correlate to tissue composition, and hence to disease state. However, when comparing the two wave modes in terms of clinical applicability for elasticity imaging, shear waves have been preferred for tissue characterization because: (i) their wave propagation speed has a larger range compared to longitudinal waves (speed range of 0.5-20m/s vs. 1350-1700m/s in soft tissues (8)) making it easier to distinguish differences in speed; (ii) their wave propagation speed is elevated by pathological changes (up to two orders of magnitude (13)) and (iii) tissue Doppler echography with a frame rate in the order of kHz can be used to track shear waves .

Shear wave speed estimation in a thin-walled viscoelastic medium such as the cardiac wall is not straightforward as a shear wave of a finite temporal length intrinsically contains a range of frequencies – as an ultrasound pulse – and these frequencies can travel at different speeds, a phenomenon which is called *velocity dispersion*. In general, there are two manners to characterize the propagation of a wave: the phase and the group velocity (14). The phase velocity is the speed with which a given frequency component of the waveform propagates, whereas the group velocity is the speed with which the envelope of a pulse within a frequency band propagates as illustrated in Figure 2b (14). The distinction between both speed types is important, as both speed estimations are often used interchangeably in cardiac SWE for diagnosis while phase velocity in general does not match with group velocity in the cardiac wall for current SWE-techniques.

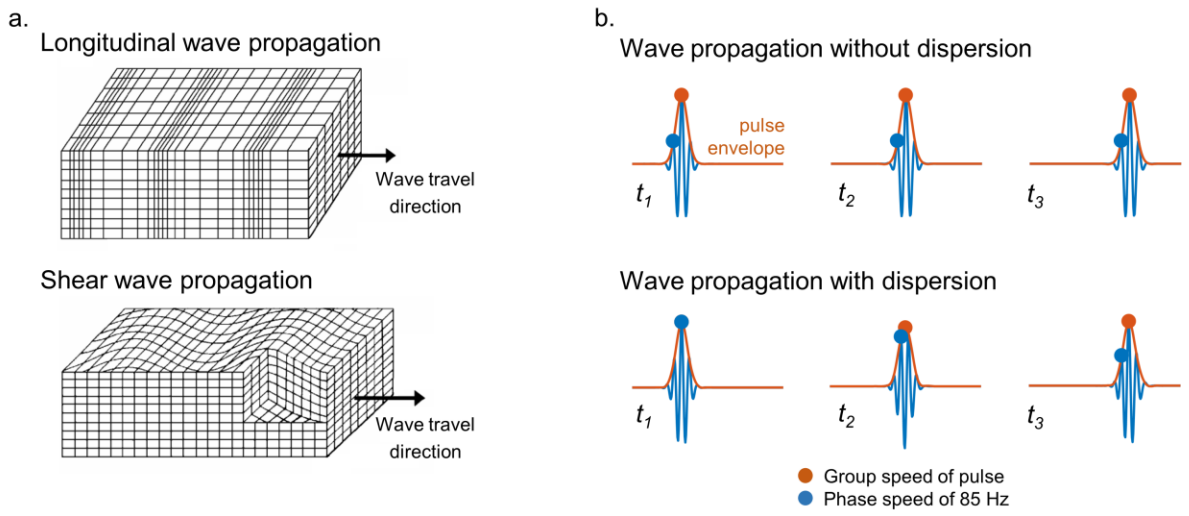

Figure 2 – Basic wave physics principles. (a) Direction of the tissue motion and wave propagation for longitudinal and shear wave propagation (adapted from (8)). (b) Concept of group and phase speed. Individual waves with a specific frequency propagate at the phase velocity (blue dot); whereas the pulse envelope propagates at the group velocity (orange dot).

Cardiac ultrasound shear wave elastography

Shear wave excitation sources

SWE can be realized in different manners, where the source of excitation of the shear waves is an important distinguishing criterion for cardiac SWE (see also Figure 3 and Table 1):

- Acoustic radiation force (ARF): by applying a high-intensity focused US beam for a relatively long period of time but still in an impulsive manner (< 1 ms), a localized body force is generated of a sufficiently large magnitude to evoke particle displacements in the order of a few micrometers in the direction of the US beam (15-17). In other words, the US beam literally pushes the tissue away from the transducer, while the transducer is at a distance. For cardiac SWE, the geometrical shape of the ARF is typically ellipsoidal around the US beam axis with a length encompassing the thickness of the cardiac wall (using a strongly focused US beam or a low emission frequency). The wall region of interest should be oriented parallel with the transducer surface such that the “push” excites mainly transverse motion, which is a condition best met in the parasternal long or short axis (PLAX/PSAX) view of the interventricular septal wall for transthoracic closed-chest settings, but more non-conventional views are feasible in an open-chest setting.
- Intrinsic motion (natural waves): mechanical waves are also caused by fast transient events in the heart such as valve closure. Previous research mainly focused on the mechanical wave propagation in the left ventricle after mitral and aortic valve closure (MVC, AVC) (18,19) but also after atrial kick (AK) (20). As the spatial and temporal properties of the excitation source are unknown, the understanding of the measured phenomena remains poor. A recent 3D study on natural waves (21) has shown that there might be two sources of wave excitation after MVC, but these results are still very preliminary (n=3). Natural waves after valve closure contain both transversal and

longitudinal components of tissue motion, explaining why analyses based on both parasternal and apical views have been reported in literature (12,22). Mechanical waves following AK did not reveal any wave-like pattern in the parasternal view, suggesting that AK's wave motion is predominantly longitudinal (23) and therefore this wave phenomenon is not further considered in this review.

- External mechanical actuator: some preclinical studies (24,25) reported the use of an actuator vibrating at a specific frequency to induce a monochromatic (i.e. single frequency) mechanical wave. This procedure is then repeated for multiple vibration frequencies such that the frequency behavior of the shear wave can be studied. This method has only been reported in open-chest studies (26) for ultrasonic SWE, but this excitation method is typically used in magnetic resonance elastography (27) and harmonic ultrasound elastography (28).

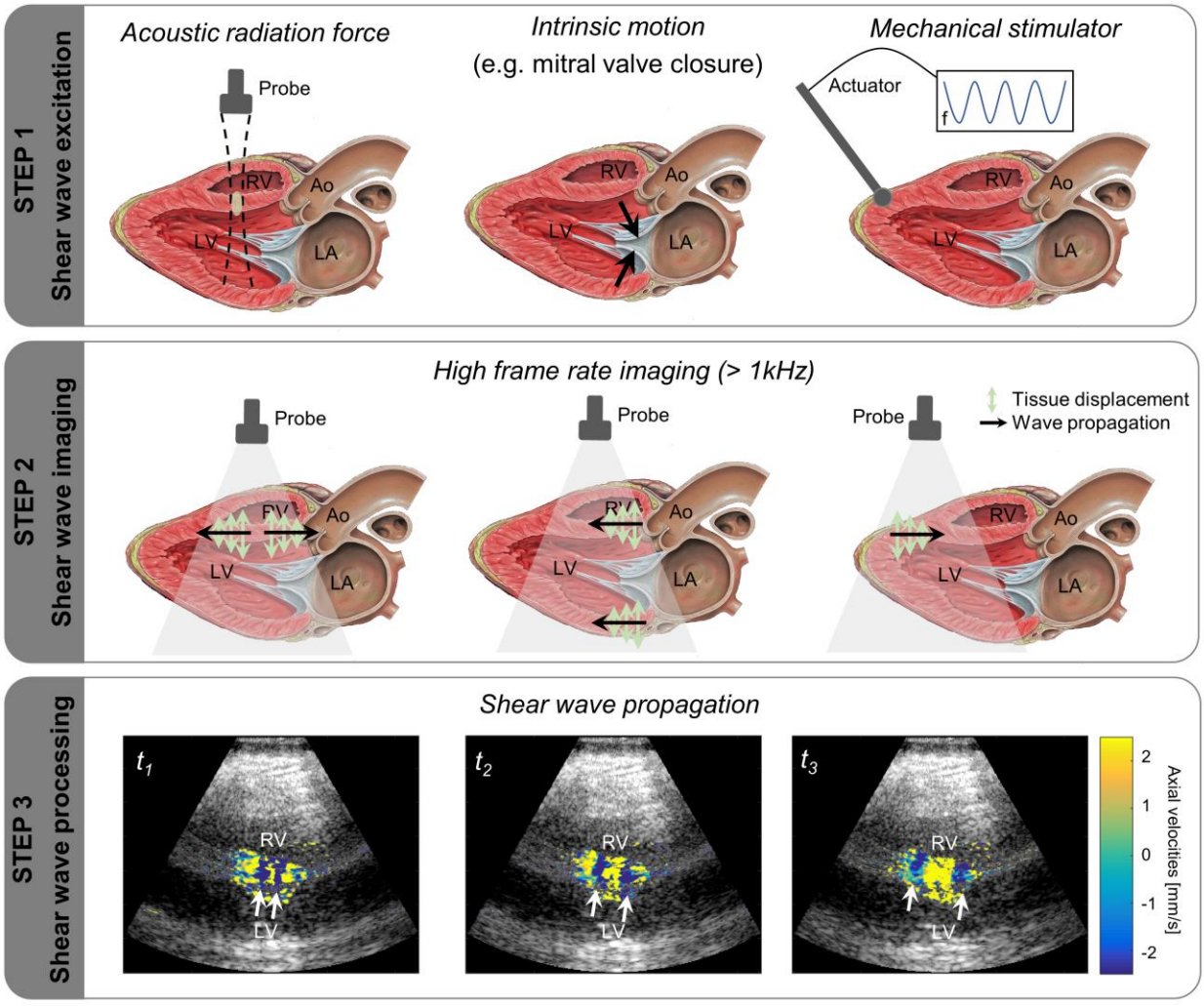

Figure 3 – Principle of ultrasound SWE in a cardiac setting (anatomical image adapted from (29)). Shear wave propagation shown as example in step 3 is measured in vivo in the interventricular septum of a closed-chest pig using an acoustic radiation force for shear wave excitation in an ongoing study (approved by the Ethical Committee for Animal Experiments of KULeuven P041/2019).

It should be noted that mechanical waves after valve closure occur at specific locations and moments in the cardiac cycle, whereas an ARF-induced shear wave is in theory fully controllable in time and space by the user, as much as the acoustic windows allow for. However, transthoracic excitation of shear waves in an acoustically safe manner remains challenging due to the limited aperture size (small acoustic windows) and small amplitude and quickly attenuating tissue motion in especially the stiff cardiac wall in systole. The use of intracardiac (30) or trans-esophageal (31) transducers might offer a solution to this problem, but this comes with patient discomfort, increased health risks, and demanding technical requirements – small piezoelectric elements with enough power to generate a sufficiently large ARF. An advantage of intrinsic mechanical waves is their displacement magnitude which is one order of magnitude larger than that of ARF-induced waves (Table 1), improving the signal-to-noise ratio (SNR) of SWE. Additionally, transthoracic imaging of natural waves does not pose any problems regarding acoustic safety, permitting an easy implementation in clinical practice.

Table 1 – Overview of different wave excitation sources in ultrasonic cardiac SWE with typical application settings and shear wave properties (IVS: interventricular septum; LVW: left ventricular wall; LVFW: left ventricular free wall; NR: not reported; PLAX: parasternal long-axis view; PSAX: parasternal short-axis view).

	Excitation source	**Timing**	**Frequency content**	**Tracked tissue motion**	**Cardiac wall location**	**Reported metrics**
Open/closed-chest	Acoustic radiation force (impulsive)	Any instant in cardiac cycle*	<500 Hz (32)	Transversal ~ 5 µm (15)	IVS in PLAX/PSAX LVFW (open-chest)	Group speed (33) Elasticity (34) Group speed (35,36) Group speed, elasticity, viscosity (26)
	Intrinsic motion	AVC/MVC	<150 Hz (18,37,38)	Transversal ~ 100 µm (18,19) Longitudinal	Mainly IVS in PLAX IVS in AP3C/AP4C (12,22)	Group speed (19,39,40) Group speed, phase speed (18) Phase speed, elasticity, viscosity (37)
Open-chest	External vibrator	Any instant in cardiac cycle	50-400 Hz in steps of 50 Hz (25)	Transversal 10-100 µm (25)	LVFW	Phase speed, elasticity, viscosity (24,25)

* Very low success rate in systole.

Shear wave imaging and reconstruction of shear wave speed maps

High frame rate imaging (frame rate >500 Hz) is applied to visualize the propagating shear wave. The use of diverging wave imaging in a fundamental (19) or pulse-inversion harmonic (41) manner has been reported for this purpose. Spatial resolution and contrast can be further improved by coherently compounding diverging waves emitted from multiple angles (42) or zones (19). After recording the shear wave motion, a tissue motion estimator is applied to the radio-frequency (RF) or demodulated in phase quadrature (IQ) data (e.g. a standard Doppler auto-correlator as the one described by Kasai et al. (43)).

For shear wave speed estimation, the first step is to select a wave propagation path along the cardiac wall which also includes the shear wave excitation source (white line in Figure 4a). The

excitation source is always included in the imaging plane for ARF-induced waves as the same transducer is used to generate and detect shear waves, but attention should be paid to include the valves in the imaging plane when visualizing waves after intrinsic motion (3). A curved (anatomical) M-mode displaying tissue motion data as a function of space and time is then obtained, as illustrated in Figure 4b. Various methods have been reported in literature to distinguish the high frequency wave motion from the low frequency gross cardiac motion in this M-mode: application of a high-pass filter on tissue motion data (18,40) (example is shown in Figure 4b-c) or on the IQ data (39), subtraction of the average wall motion (44) or representation of tissue motion in the form of accelerations (19). Shear wave speed estimation is then typically performed using a time-of-flight (TOF) estimator, which characterizes the shear wave's position as a function of time (see Figure 4c). The resulting speed can be classified as *phase speed* when using a single frequency source (external vibrator in Table 1), and as *group speed* when using a broadband excitation (ARF/intrinsic motion in Table 1) (45). Note that the *phase speeds* of all excited frequencies in the shear wave motion can be studied by repeating the measurement at a different frequency in case of an external vibrator or performing a Fourier analysis in the frequency domain in case of ARF/intrinsic motion (*velocity dispersion analysis* (46)). Most studies report shear wave speed as an end result, whereas others convert speed c_T into Young's modulus E through equation (1) and the following equation:

$$E = 2(1 + \nu)\mu \approx 3\mu \tag{2}$$

with Poisson's ratio ν (usually assumed 0.5 to describe tissue incompressibility (7)). Note that application of equation (2) implies that the myocardium is a priori considered an isotropic linear elastic material, and all observed wave phenomena are analyzed and interpreted within that paradigm. Unfortunately, this is an over-simplification, and it remains poorly understood how the conversion to true stiffness constants can be made accurately for the myocardium.

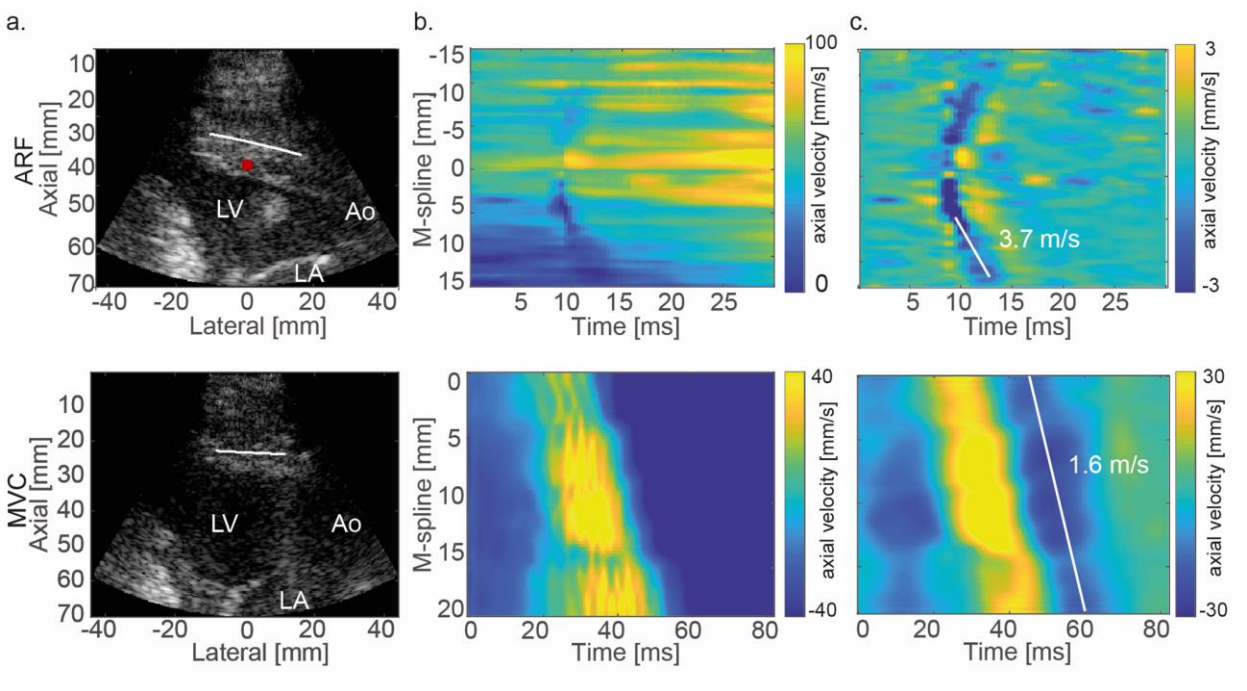

Figure 4 – Reconstruction of shear wave speed. (a) B-mode in parasternal long-axis view for acoustic radiation force (ARF) induced shear waves in the upper panel (red rectangle indicates push focus) and shear waves induced by mitral valve closure (MVC) in lower panel. (b) Measured tissue motion. (c) Measured shear wave motion after application of band pass filter with cut-off frequencies at 75-750 Hz for ARF-induced wave and 15-100 Hz for MVC-induced wave. For ARF-based SWE, two shear waves are created in the center of the field of view (in the IVS); whereas for natural SWE one shear wave is propagating from base to apex. Adapted with permission from Keijzer and Caenen et al. (33).

Recently, 3D high frame rate approaches have been reported in cardiac SWE through the use of ECG stitching (47) or coupling multiple US systems (21). Both approaches have been applied for imaging natural waves for which the wave propagation physics is less well defined than for ARF-induced waves. These 3D approaches allow to first apply a wave excitation source localization method to determine the wave propagation path for local wave speed estimation using a TOF algorithm.

Mechanical factors affecting shear wave speed in the heart – what causes complexity?

The interpretation of measured shear waves in the heart is complex due to multiple mechanical factors directly affecting shear wave speed values and interfering with effects of pathology. In this section, we review how geometry, viscosity, anisotropy, contraction/relaxation, hemodynamics, and pathology affect shear wave patterns and speed (Figure 5). We first macroscopically describe the effect of each factor on shear wave propagation and summarize its impact on reported wave speed variations in Table 2. Diastolic and systolic speeds are reported in separate columns, with the speed of the mechanical waves after MVC and AVC classified as diastolic and systolic speed, respectively (even though this classification is debatable as in some definitions the diastolic and systolic phases are ending at the moment of valve closure).

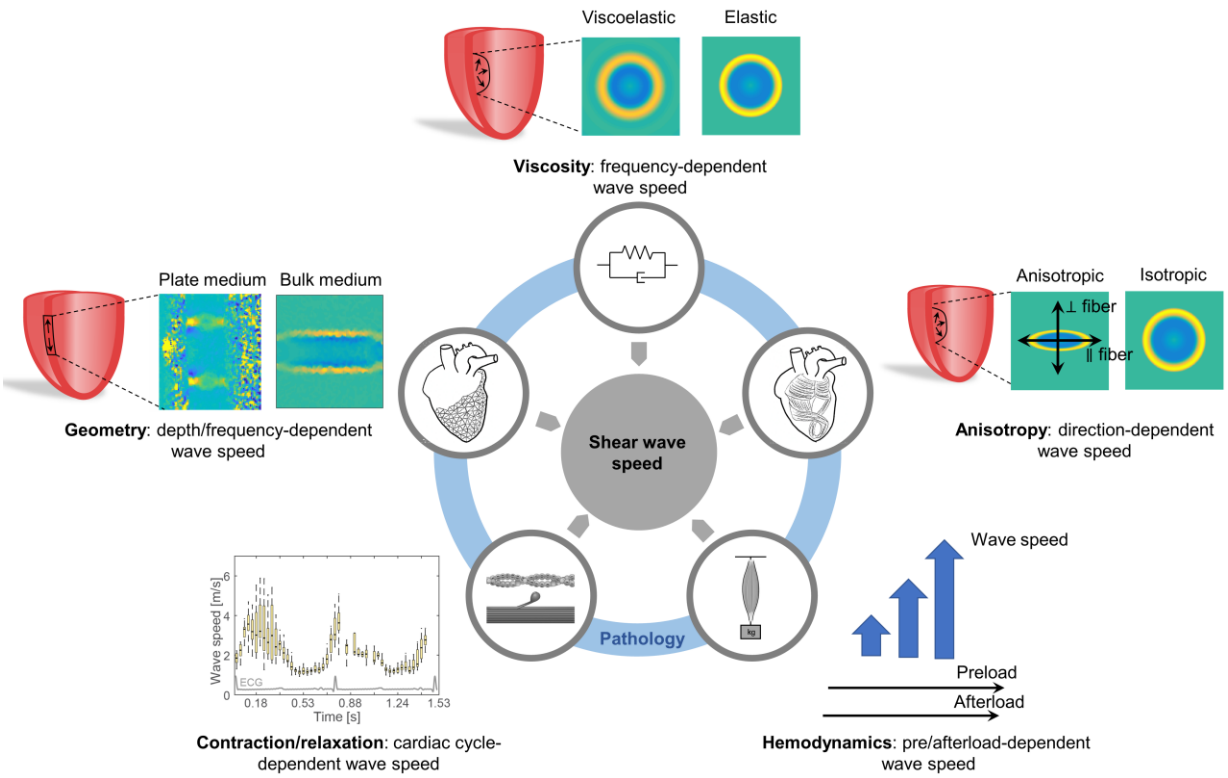

Figure 5 – Mechanical factors affecting wave speed estimation in cardiac shear wave elastography.

Geometry

Pure shear waves theoretically only exist in an infinite medium, a condition that is sufficiently met when the shear wavelength is significantly smaller than the smallest dimension of the medium in which it travels. In general, the studied wavelength in cardiac SWE depends on the selected excitation source (see Table 1), typically a few mm for ARF-induced waves and a few cm for natural waves, which is of the same order of magnitude or larger than the cardiac wall thickness (24-26,37). This means that the wave will reflect from the boundaries, confining the mechanical energy within the wall (Figure 6a) leading to guided waves. The wave front might be visually distorted during propagation (Figure 6b), potentially resulting in a depth-dependent shear wave propagation speed as visualized in Figure 6b for a left ventricular phantom. Also, the wave guide can result in dispersive effects, with the phase speed increasing as a function of frequency, as illustrated in Figure 6b and tabulated in Table 2 (14). The nature of the shear wave is thus altered and consequently the propagation characteristics are not only dependent on stiffness – as one would conclude from equation (1) – but also on geometry, tissue surrounding and excitation characteristics. LV phantom experiments and simulations have shown that the TOF method can underestimate the true stiffness up to 35% depending on wall thickness and echocardiographic view (11). The Lamb wave theory on waves in plates has been used to better understand the geometrical effect on cardiac shear wave propagation and to improve shear wave characterization methods, on which more information can be found in the appendix.

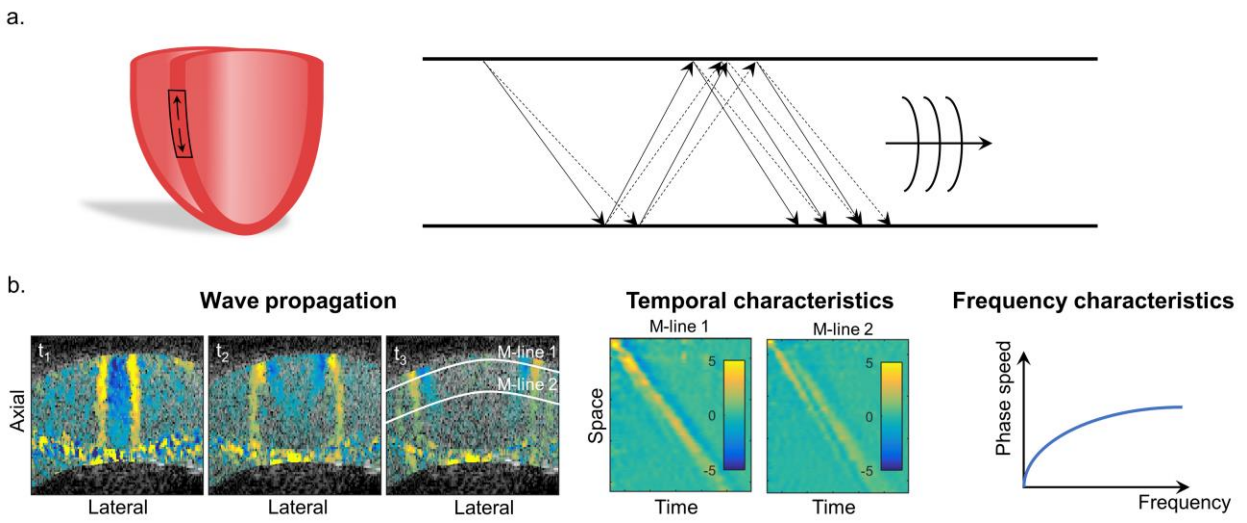

Figure 6 – Effect of geometry on shear wave properties. (a) Principle of waveguide. (b) Example of shear wave propagation in a left ventricular phantom. The two M-modes show that the shear wave propagation pattern in the time domain depends on the chosen depth. The frequency characteristics demonstrate an increasing phase speed as a function of frequency. Adapted with permission from Caenen et al. (11).

Viscosity

Viscosity leads to absorption of the mechanical wave energy due to viscous friction, resulting in attenuation of the wave's amplitude. The viscosity-related attenuation increases with frequency, leading to a smoothed wave shape by removal of the high frequencies as shown in the Figure 5 (48). This comes together with an apparent stiffening of the material with increasing frequency, which in turn leads to a frequency-increasing phase velocity, as is conceptually illustrated in Figure 7. The range of speeds that is reported by various studies is summarized in Table 2. Often a linear dispersion model is assumed (the so-called Voigt model, showing a linear dependence of phase speed on frequency as visualized in Figure 7), but in reality the frequency characteristics will rather behave as demonstrated in Figure 6b. Some studies used this frequency-dependency to estimate myocardial viscoelasticity (24-26,37), which might provide additional diagnostic value next to elasticity (49). For further details on this type of material characterization, we refer the reader to the appendix.

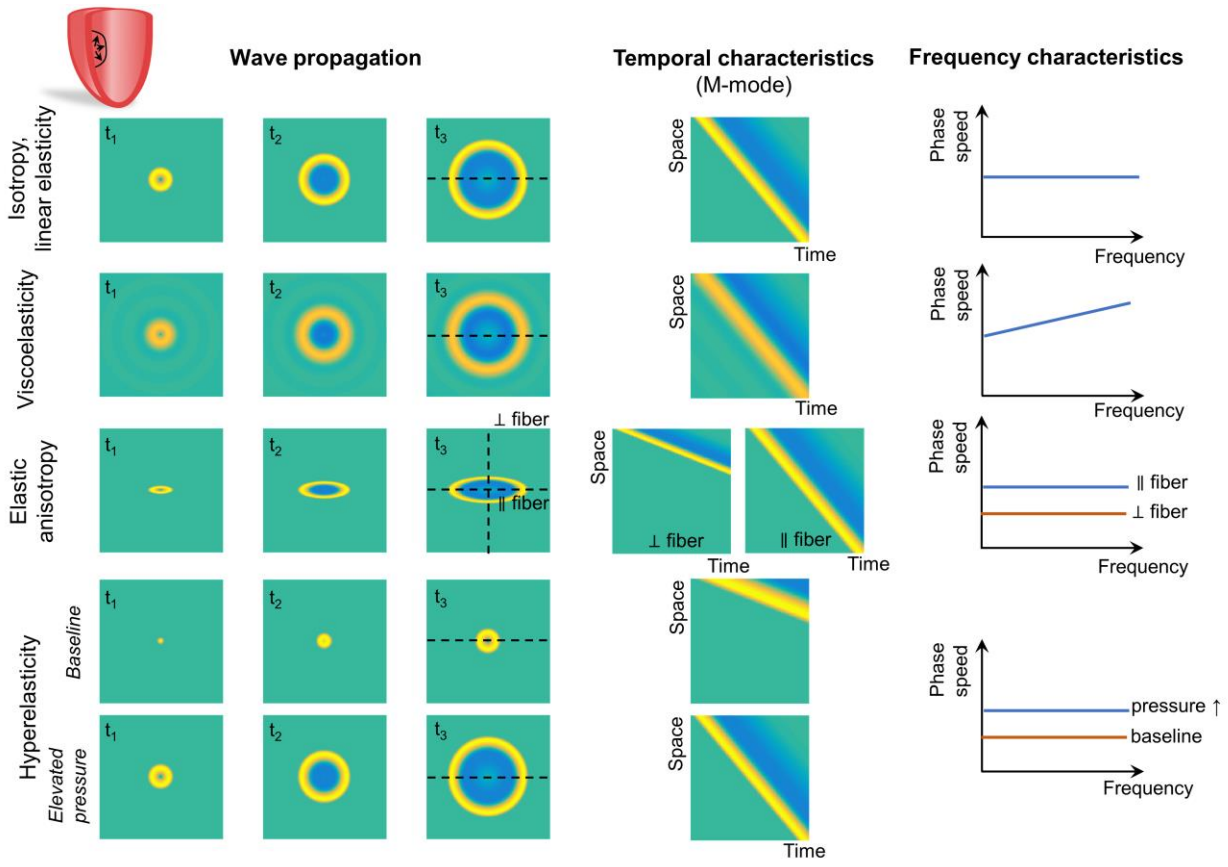

Figure 7 – Conceptual representation of the effect of viscoelasticity, elastic anisotropy and hyperelasticity on shear wave propagation, temporal and frequency characteristics.

Anisotropy

It is known from physics that shear waves propagate faster along the fiber than across due to elastic anisotropy, resulting in an elliptical shaped propagation pattern (9) (see Figure 5 and Figure 7). The myocardial fiber architecture is however complex: it follows a helical arrangement and it varies transmurally. For the sake of simplicity, however, many studies have assumed that the myocardium is locally transverse isotropic, with a symmetry axis along the local direction of fiber, resulting in a transmural varying wave directionality parallel to the cardiac wall (see Figure 8a and Table 2). This anisotropy in shear wave propagation can be assessed by analyzing the transmural wave speed variations in 3D (see Figure 8b) or in two echocardiographic views (Figure 8c). For example, wave speed in PSAX is higher than in PLAX at the mid cardiac wall for both ARF-induced (34) and natural waves (21). Some studies have used this anisotropy in wave propagation to extract the myocardial fiber orientation, which agreed well with histology (50) and magnetic resonance diffusion tensor imaging (51). Other studies suggest that anisotropy of wave propagation offers additional diagnostic value (34). In that respect, Couade et al. (35) introduced a new parameter, called *fractional anisotropy* (FA), to estimate the degree of anisotropy:

$$FA = \frac{\sqrt{(v_{PSAX} - \bar{v})^2 + (v_{PLAX} - \bar{v})^2}}{\sqrt{v_{PSAX}^2 - v_{PLAX}^2}} \quad (3)$$

With v_{PSAX} the speed in PSAX, v_{PLAX} the speed in PLAX and $\bar{v}$ the average of v_{PSAX} and v_{PLAX}. FA can be calculated at any transmural depth, as shown in Figure 8c for the LV free wall in an open-chest sheep in diastole and systole (35). Villemain et al. (34) reported a FA of 0.238±0.068 for the mid cardiac wall in healthy volunteers, and a decreased FA of 0.133±0.073 in patients with hypertrophic cardiomyopathy (HCM).

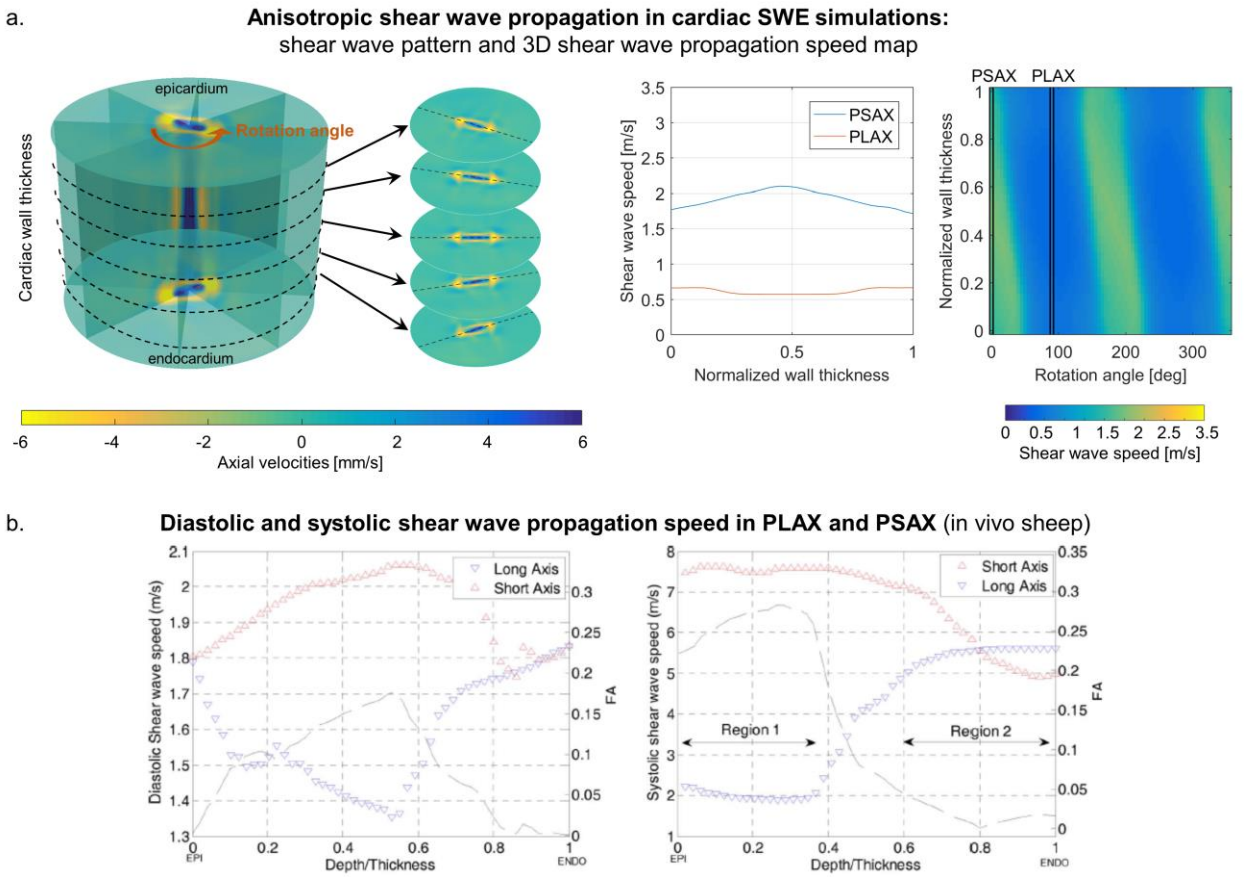

Figure 8 – Effect of anisotropy on shear wave properties for ARF-induced shear waves. (a) Demonstration of the ellipsoidal wave propagation patterns for various slices across cardiac wall thickness in a computer model of cardiac SWE (52). The black dotted line in the slices represents the actual myocardial fiber orientation in the model. A shear wave propagation speed map can be obtained when analyzing the wave propagation for every angle in each transmural slice. The maximal speed in this map corresponds approximately to the myocardial fiber orientation (52). Adapted with permission from Caenen et al. (52). (b) Transmural shear wave speed and fractional anisotropy variations in diastole and systole of the LVFW of an open-chest sheep. Adapted with permission from Couade et al. (35).

Contraction/relaxation

Besides passive material properties, cardiac contraction affects shear wave speed measurements (see Table 2), providing opportunities for assessing time-varying muscle stiffness and, hence, myocardial contractility. Indeed, Bézy et al. (53) found a positive linear correlation

between the wave speed after AVC and end-systolic elastance ($R=0.640$; $p<0.001$) after dobutamine administration and bicycle exercise. Application of ARF-based SWE in a Langendorff animal heart set-up allowed to relate the shear wave speed in systole to the inotropic state of the heart in an unloaded condition: systolic stiffness was linearly correlated to coronary perfusion pressure (0.27 kPa/mmHg; $R^2=0.73$ (54)) and to systolic pressure during administration of isoproterenol ($R^2=0.94$-0.98; $p<0.0001$ (55)). Furthermore, repeated application of ARF-based SWE throughout the cardiac cycle allows to capture the dynamic stiffness variations (see Figure 9c). Two studies of the same authors (56,57) have used the wave speed variations during the isovolumic relaxation phase to estimate the relaxation time constant of diastolic function. The researchers reported an average time constant of 65±19 ms for 8 Langendorff perfused rabbit hearts, which increased to 154±60 ms after MI induction. Furthermore, a linear regression model demonstrated the similarity between the relaxation time constant obtained from the LV pressure curve and the ARF-based shear wave speed curve (slope=1.164; $R^2=0.8$ (56)).

It should, nonetheless, be noted that the timing of the mechanical waves after valve closure within the isovolumic contraction/relaxation phase is unclear. Recent work combining ARF-based and natural SWE (33) was able to detect both wave types in the same acquisition as visualized in Figure 9a and b. This permitted to investigate the timing of natural wave measurements with respect to ARF-assessed cardiac dynamics: waves after valve closure occurred when the myocardium is in between relaxation and contraction (Figure 9c). Additionally, this figure shows a good match in propagation speeds between natural and ARF-based SWE at the moment of valve closure, despite the clear differences in wavelength (a few mm vs. a few cm) and wave amplitude (a few mm/s vs. tens mm/s) (Figure 9a-b). This result shows that many factors, such as fluid loading, contraction speed, contraction synchronicity, or even stenosis of outflow track or mitral valve, can affect the exact moment of valve closure, and hence the instantaneous speed of the induced wave.

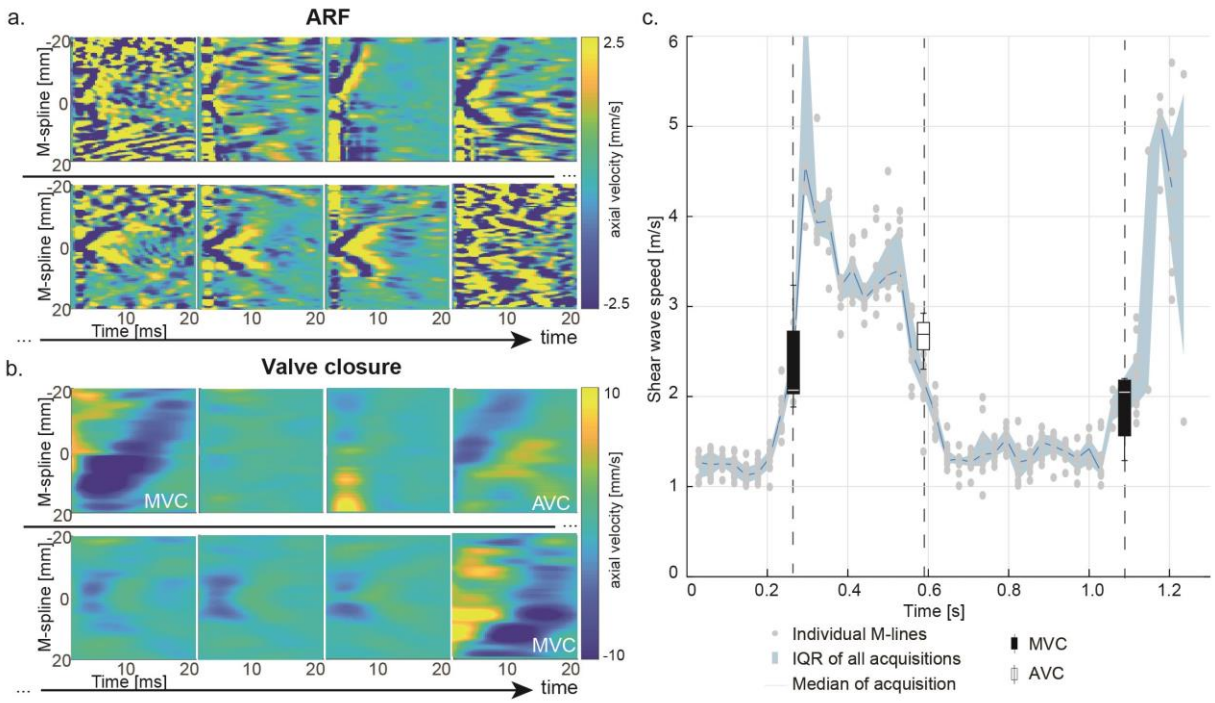

Figure 9 – Shear wave propagation throughout the cardiac cycle in a pig's septal wall. Two types of shear waves are visible in the same SWE acquisition: shear waves induced with an acoustic radiation force (ARF; panel a) and by valve closure (VC; panel b). Panel c demonstrated the estimated shear wave speeds for both techniques. Adapted with permission from Keijzer and Caenen et al. (33).

Hemodynamics

Altering preload or afterload affects the magnitude of the pressure acting on the cardiac wall, and thus the stress/strain state in the ventricle because of the material's hyperelasticity (see Figure 1b and Figure 7). Table 2 quantifies the effect of changing loading condition on the wave speeds. A negligible change in diastolic wave speed was reported for ARF-based SWE (Δ0.04 m/s for ΔEDP of 14.7 mmHg (55) and Δ0.5 kPa for ΔEDP of 5 mmHg (25)), whereas the wave speed after MVC increased significantly with increased EDP (Δ4.9 m/s for ΔEDP of 21.7 mmHg: $r=0.83$ and $p<0.001$ (58)). Differences in shear wave excitation properties, experimental set-up and investigated pressure range partly explain the reported difference in the sensitivity of shear wave speed to pressure, but more importantly, the end-diastolic moment of the shear wave recording for ARF-based SWE might still be in the quasi-linear part of the stress-strain relationship whereas this might be different for the shear wave after MVC for which, again, the exact timing within the isovolumic contraction phase is unclear (33,38).

Pathology

Most literature on SWE in pathology is obtained in animal models (25,35,44) by inducing a myocardial infarction (MI) through ligation of a coronary artery using ARF-based SWE. Studies have consequently reported an increase in diastolic wave speed following MI (range of Δ0.11-2.18 m/s for all studies; Table 2), of which its magnitude depended on the duration of ligation (15-120 minutes) and reperfusion (40-120 minutes). A short term ligation of 15 minutes did not affect

diastolic wave speed permanently (35,44). The increase in diastolic wave speed after MI was validated, by comparison with several invasive measurements: (i) an increase in the exponential coefficient of the end-diastolic pressure volume relationship (4.027 vs. 2.010 ml^{-1}) (56), (ii) an increase in the exponential coefficient of the end diastolic strain-stress relationship measured with sonomicrometry (25.7±9.5 vs. 8.8±2.3) (44) and (iii) an increase in the shear modulus obtained with the pressure-segment length method (9.4±4.9 kPa vs. 1.9±0.5 kPa) (25). Fewer studies (25,35,59) also investigated the effect of MI on systolic wave speed, but the results are inconclusive.

Cardiac pathology might be associated with other changes next to an increased wall stiffness such as an increased wall thickness (hypertrophy), a change in viscosity and fiber disarray – especially when tissue remodeling and fibrosis occurs. Conceptually, more parameters than shear wave speed are necessary to completely describe the effect of pathology, but the clinical relevance of additional parameters needs further investigation. For example, Pislaru et al. (25) showed an increase in elasticity and viscoelasticity at end-diastole after reperfusion, whereas less consistent changes were found during systole.

Table 2 – Overview of (pre)clinical feasibility studies that have investigated the effect of one or more mechanical factors on wave propagation speed (ARF: acoustic radiation force; EDP: end-diastolic pressure; ESP: end-systolic pressure; FFT: fast Fourier transform; ICE: intracardiac echocardiography; LAD: left anterior descending coronary artery; LCX: left circumflex coronary artery; MI: myocardial infarct; MS: mechanical stimulation; VC: valve closure; LVFW: left ventricular free wall; other abbreviations are as listed in Table 1).

	Study description (ref #)	**Study set-up/results**				
		Excitation	**Region**	**Species**	**Diastolic wave speed**	**Systolic wave speed**
Geometry & viscoelasticity	Analyze frequency content using FFT (26)	ARF	LVFW	Open-chest pig (n=1)	NR	2.2 m/s at 100 Hz to 4.8 m/s at 500 Hz
	Determine phase speed at various frequencies (24)	MS	LVFW	Open-chest pigs (n=8)	1.1±0.2 m/s at 50 Hz 1.5±0.3 m/s at 100 Hz 1.6±0.4 m/s at 150 Hz 1.7±0.2 m/s at 200 Hz 2.1±0.5 m/s at 250 Hz 2.4±0.4 m/s at 300 Hz 2.5±0.5 m/s at 350 Hz	3.2±0.9 m/s at 50 Hz 3.0±0.6 m/s at 100 Hz 3.3±0.5 m/s at 150 Hz 3.8±0.6 m/s at 200 Hz 4.2±0.6 m/s at 250 Hz 4.5±0.9 m/s at 300 Hz 5.0±1.2 m/s at 350 Hz
	Determine phase speed at various frequencies (25)	MS	LVFW	Open-chest pigs (n=10)	1.4±0.4 m/s at 100 Hz 1.5±0.5 m/s at 150 Hz 1.6±0.2 m/s at 200 Hz 2.1±0.5 m/s at 250 Hz 2.4±0.3 m/s at 300 Hz 2.5±0.5 m/s at 350 Hz	3.1±0.5 m/s at 100 Hz 3.8±1.6 m/s at 150 Hz 4.4±2.0 m/s at 200 Hz 4.1±0.6 m/s at 250 Hz 4.4±1.0 m/s at 300 Hz 4.8±1.3 m/s at 350 Hz
	Analyze frequency content using FFT (37)	VC	IVS	Human (n=5)	NR	1-2 m/s at 20 Hz 3-4 m/s at 50 Hz 3-7 m/s at 90 Hz
	Analyze frequency content using FFT (18)	VC	IVS	Pig (n=22)	2.0 m/s at 15-45 Hz 2.6 m/s at 45-75 Hz 3.8 m/s at 75-110 Hz 3.4 m/s at 110-150 Hz	3.8 m/s at 15-45 Hz 3.8 m/s at 45-75 Hz 4.4 m/s at 75-110 Hz 4.1 m/s at 110-150 Hz
Anisotr	Analyze different depths and views (35)	ARF	LVFW	Open-chest sheep (n=10)	Mid: 1.45±0.32 m/s in PLAX; 1.85±0.22 m/s in PSAX Epi: 1.8 m/s in PLAX and PSAX	Mid: 4.8±1.4 m/s in PLAX; 6.2±1.9 m/s in PSAX Epi: 2.2 m/s in PLAX; 7.4 m/s in PSAX

					Endo: 1.8 m/s in PSAX and PSAX	Endo: 5.7 m/s in PLAX; 5.0 m/s in PSAX
	Analyze PSAX and PLAX (34)	ARF	IVS	Human (n=60)	1.54±0.26 m/s in PLAX 2.16±0.42 m/s in PSAX	NR
	Analyze different axial and lateral locations (36)	ARF	LVFW	Open-chest dog (n=1)	0.82-2.65 m/s depending on location	NR
	Analyze different axial and lateral locations (60)	VC	IVS	Open-chest pigs (n=3)	NR	5.7-10.1 m/s depending on location
	Analyze wave propagation in 3D (21)	VC	IVS	Human (n=3)	2.8±0.5 m/s in PLAX 4.6±0.7 m/s in PSAX	3.4±0.1 m/s in PLAX 3.5±0.3 m/s in PSAX antero-septal 5.4±0.7 m/s in PSAX postero-septal
Contraction/relaxation	Administer isoproterenol (10^{-8} mol/l) (55)	ARF	LVFW	Langendorff rat (n=6)	NR	*Pre: 3.18 m/s* *Post: 4.84 m/s*
	Changing Krebs extracellular calcium concentration (55)	ARF	LVFW	Langendorff rat (n=6)	*0.8 mMol: 1.00 m/s* *1.8 mMol: 1.01 m/s* *2.5 mMol: 1.01 m/s*	*0.8 mMol: 1.66 m/s* *1.8 mMol: 2.95 m/s* *2.5 mMol: 3.61 m/s*
	Alter coronary perfusion pressure (0-90 mmHg) (61)	ARF	LVFW	Langendorff rabbit (n=8)	1.36±0.08 m/s at 0 mmHg 1.58±0.05 m/s at 25 mmHg 1.84±0.05 m/s at 50 mmHg 2.03±0.05 m/s at 75 mmHg 2.34±0.15 m/s at 90 mmHg	NR
	Alter coronary perfusion pressure (0-90 mmHg) (54)	ARF	LVFW	Langendorff rabbit (n=12)	NR	*3.16 m/s at 0 mmHg* *4.09 m/s at 25 mmHg* *4.85 m/s at 50 mmHg* *5.50 m/s at 75 mmHg* *5.86 m/s at 90 mmHg*
	Perform dobutamine stress test (19)	VC	IVS	Human (n=1)	Pre: 2.9 m/s 10 µg/(kg·min): 15.5 m/s 40 µg/(kg·min): 19.7 m/s	NR
	Perform supine bicycle exercise test (66% work load) (53)	VC	IVS	Human (n=11)	NR	Pre: 3.3±0.5 m/s Post: 6.2±1.7 m/s
	Perform dobutamine stress test (53)	VC	IVS	Human (n=9)	NR	Pre: 4.4±0.6 m/s 40 µg/(kg·min): 7.2±1.7 m/s
Hemodynamics	Increase preload (EDP: 5.8±0.7 to 20.5±6.9 mmHg; ESP: 72±7.4 to 124.7±13.5 mmHg) (55)	ARF	LVFW	Langendorff rat (n=6)	*Pre: 1.30 m/s* *Post: 1.34 m/s* (Δ +0.04 m/s)	*Pre: 3.18 m/s* *Post: 3.51 m/s* (Δ +0.33 m/s)
	Reduce preload (ΔEDP= -10.1±2.5 mmHg) (58)	VC	IVS	Pigs (n=5)	Δ -1.2±1.4 m/s	NR
	Increase preload (ΔEDP= +2.3±2.7 mmHg) (58)	VC	IVS	Pigs (n=5)	Δ +2.0±0.8 m/s	NR
	Increase afterload (ΔEDP=+2.3±2.1 mmHg) (58)	VC	IVS	Pigs (n=5)	Δ +1.9±0.7 m/s	NR
Pathology	Induce MI by 1-3h ligation of mid to distal LAD and 1-2h reperfusion (25)	MS	LVFW	Open-chest pigs (n=10)	2.7±1.0 m/s at 100 Hz 2.9±0.7 m/s at 150 Hz 3.3±1.3 m/s at 200 Hz 3.5±1.1 m/s at 250 Hz 3.4±0.6 m/s at 300 Hz 3.4±0.8 m/s at 350 Hz	5.4±2.4 m/s at 100 Hz 4.6±1.4 m/s at 150 Hz 4.8±0.8 m/s at 200 Hz 5.6±0.6 m/s at 250 Hz 5.0±0.6 m/s at 300 Hz 5.6±1.0 m/s at 350 Hz

	Induce MI by 2h ligation of LAD diagonal branch and 2h reperfusion (44)	ARF	LVFW	Open-chest sheep (n=10)	*Pre: 1.30 m/s* *Post MI: 2.49 m/s* *Post reperfusion: 3.48 m/s*	NR
	Induce MI by 15 min ligation of LAD diagonal branch and 40 min reperfusion (44)	ARF	LVFW	Open-chest sheep (n=10)	*Pre: 1.34 m/s* *Post MI: 1.45 m/s* *Post reperfusion:1.52 m/s*	NR
	Induce MI by 20 min ligation of LAD (35)	ARF	LVFW	Open-chest sheep (n=1)	Pre: 1.3±0.1 m/s Post MI: 1.46±0.1 m/s	Pre: 6.0±0.2 m/s Post MI: 1.3±0.1 m/s
	Induce global MI by stopping inflow perfusion for 10 min and re-perfuse heart for 10 min (56)	ARF	LVFW	Langendorff rabbit (n=11)	*Pre: 2.31 m/s* *Post MI: 3.25 m/s*	NR
	Induce MI by ligating LAD and LCX for 130±24 days (59)	ARF (ICE)	IVS	Pigs (n=4)	Pre: 1.414±0.102 m/s Post MI: 1.444±0.059 m/s	NR

Derived from graph or calculated from text

Converted from stiffness to shear wave speed by assuming ρ of 1000 kg/m^3

Clinical application

Shear wave speeds in healthy volunteers and patients

Various clinical studies have confirmed that mechanical factors do affect shear wave speed, and should be considered when interpreting SWE data. An overview is given in Table 3. Indeed, shear wave speed has been shown to significantly and positively correlate with ED wall thickness and with loading conditions (reflected by predictors E/e', pulmonary capillary wedge pressure, left atrial volume index or LA diameter). Additionally, a positive correlation was found between shear wave velocity and age (34,62,63).

Table 3 – Summary of reported significant correlations between shear wave speed and parameters quantifying cardiac function in various clinical studies using univariate and multivariate analyses (ED: end diastolic; EDP: end diastolic pressure; HCM: hypertrophic cardiomyopathy; HT: hypertension; HTX: heart transplantation; HV: healthy volunteer ; LA ø: left atrial diameter; LAVI: left atrial volume index; LGE: late gadolinium enhancement; LV: left ventricle; NS: not significant; PCWP: pulmonary capillary wedge pressure; other abbreviations are as listed in Tables 1 and 2).

	Study (ref #)	**Excitation**	**Patient**	**Age**	**Geometry**	**Hemodynamics**		**Pathology**
					ED wall thickness	**LA size**	**LV EDP**	
Univariate	Villemain et al. (34)	ARF	HV & HCM	R=0.881	NS	LAVI: R=0.623	E/e': R=0.783	LGE: R=0.804 T1 pre-contrast: R=0.711
	Strachinaru et al. (64)	VC	HV & HCM	NS	NR	NR	E/e': AVC: R^2=0.345 MVC: R^2=0.668	NR
	Petrescu et al. (65)	MVC	HV & amyloidosis	NR	NR	NR	E/e': R=0.74	NR
	Petrescu et al. (66)	MVC	HTX	NR	NR	NR	PCWP: R=0.54	Native T1: R=0.75
	Cvijic et al. (62)	MVC	HV & arterial HT	NR	R=0.786	LA ø: R=0.800	E/e': R=0.567	NR

	Bezy et al. (63)	MVC	HV & different cardiomyopathies	R=0.31	R=0.65	LAVI: R=0.38	E/e': R=0.50	Study group: R=0.54
Multivariate	Cvijic et al. (62): R^2=0.735	MVC	HV & arterial HT	β=0.015	NR	LA ø: β=1.353	NR	Study group: β=0.932
	Bezy et al. (63): R^2=0.55	MVC	HV & different cardiomyopathies	NR	β=0.36	LAVI: β=0.20	E/e': β=0.19	Study group: β=0.24

A summary of the reported wave speeds in literature together with aforementioned study parameters can be found in Table 4. Other relevant factors for shear wave speed interpretation are the used echocardiographic view and system (67). The manner of describing tissue motion (velocity/acceleration) is also mentioned in this table, as this affects the wave's frequency content and consequently the wave speed through dispersive effects (68). Table 4 shows higher speeds for waves after MVC and AVC than for ARF-induced waves at end-diastole. However, it is difficult to interpret the absolute speed values of both techniques since their timing and wave nature might be different (see Figure 9). Wave speeds in patients were in general higher than those in healthy volunteers.

Table 4 – Overview of reported shear wave speed values in healthy volunteer and patient studies with n≥10. For SWE based on intrinsic motion, speeds at MVC are tabulated as diastolic speeds and speeds at AVC are denoted as systolic speeds (abbreviations are as listed in Table 1, 2 and 3). In the column 'motion', 'a' means tissue acceleration and 'v' means tissue (Doppler) velocity are used for wave speed estimation.

		Study (ref #)	Population						System	Motion	Region	View	Wave speeds	
			n	Age [yrs]	ED wall thickness [mm]	LAVI [ml/m^2]	LA ø [mm]	E/e'					Diastole [m/s]	Systole [m/s]
Healthy volunteers	VC	Brekke et al. (22)	10	NR	NR	NR	NR	NR	GE Vingmed	a	IVS	AP4C	NR	5.41±1.28
		Keijzer et al. (12)	10	29.8±6.2	NR	NR	NR	NR	Zonare	v	IVS	PLAX/ AP4C	NR	PLAX: 3.7±0.4 AP4C: 5.7±1.8
		Keijzer et al. (40)	10	29.8±6.2	NR	NR	NR	NR	Zonare/ Philips iE33	v	IVS	PLAX	Zonare: 3.4±1.0	Zonare: 3.8±0.4 Philips iE33: 3.2±0.9
		Petrescu et al. (65)	50	37.3	10.0	26.0	NR	6.3	HD-pulse	a	IVS	PLAX	3.54±0.93	3.75±0.76
		Santos et al. (19)	30	30.9±5.1	9.1±1.4	NR	NR	NR	HD-pulse	a	IVS	PLAX	3.2 ± 0.6	3.5 ± 0.6
		Strachinaru et al. (64)	20	45±13	9±1	NR		8±1	Phillips iE33	v	IVS	PLAX	4.65±0.77	3.61±0.46
		Cvijic et al. (62)	26	55±15	10±1	31±6	33±4	6.8±1.5	HD-pulse	a	IVS	PLAX	4.04±0.96	NR
	ARF	Song et al. (69)	10	34	11.3±1.26	NR	NR	NR	Verasonics	v	IVS	PLAX/ PSAX	PLAX: 1.45±0.14 PSAX: 1.81±0.19	NR
											LVFW	PLAX/ PSAX	PLAX: 1.77±0.28 PSAX: 1.96±0.38	NR
		Villemain et al. (34)	60	50.6±16.9	5.9±1.4	25.9±8.7	NR	5.9±2.4	Aixplorer	v	IVS	PLAX/ PSAX	PLAX: 1.54±0.26 PSAX: 2.16±0.42	NR
Patients	VC	Petrescu et al. (65): amyloidosis	18	68.0	16.0	37.6	NR	18.0	HD-pulse	a	IVS	PLAX	6.33±1.63	5.63±1.13
		Strachinaru et al. (64): HCM	20	48±13	17±5	NR	NR	17±9	Phillips iE33	v	IVS	PLAX	6.88±1.22	5.13±0.68
		Cvijic et al. (62): arterial HT with hypertropic LV remodeling	33	59±14	14±2	38±10	40±7	8.8±2.7	HD-pulse	a	IVS	PLAX	5.83±1.20	NR
		Petrescu et al. (66): heart transplantation	42	54±17.8	13.3±3.1	50.2	NR	8.3±3.1	HD-pulse	a	IVS	PLAX	5.00±2.04	NR
	ARF	Villemain et al. (34): HCM	20	57±17.5	20.8±5.1	43.4±18.9	NR	16.1±6.5	Aixplorer	v	IVS	PSAX	3.56±1.71	NR

Feasibility, reproducibility and availability

For ARF-based SWE, Song et al. (69) reported good success rates (>66.7%) for four out of seven studied echocardiographic views at end-diastole (n=10): LV posterior free wall in PSAX; basal IVS in PSAX; mid-IVS in PSAX and basal IVS in PLAX. Furthermore, the first two views showed the highest repeatability across three different days. Villemain et al. (34) reported a 100% success rate when studying ARF-induced shear waves in the IVS in PLAX and PSAX (n=80) – after excluding subjects based on predefined criteria (echogenicity and presence of scar due to earlier infarct). Additionally, the authors in (34) found no statistical difference between measurements at baseline and after three months (n=15). Even though the feasibility of ARF-based SWE throughout the cardiac cycle is not yet studied in the clinics, a previous preclinical study (33) reported a success rate of 32% for 65 ARF-based SWE acquisitions (n=4). This demonstrates the SNR challenges for in vivo ARF-based SWE.

The reproducibility of natural SWE measurements in the heart has been more extensively studied. Studies report in general a high success rate (e.g. 94% for AVC and 84% for MVC for n= 63 (65)), when excluding subjects with cardiac arrhythmias, histological or clinical evidence of allograft rejection, significant LCA stenosis, more than moderate valvular disease and poor echogenicity. Healthy volunteer studies (19,40) reported a moderate reproducibility: variabilities up to 1 m/s were observed, mainly due to measurement inaccuracies such as a limited SNR and shear wave tracking length. Keijzer et al. (40) suggested to improve measurement precision by averaging wave speeds over 10 heartbeats and multiple M-mode line analyses per recording.

Most of the presented work in this review has been performed with research systems or clinical systems that have been adapted for research purposes. For ARF-based SWE, several commercial elastography functions are available from different vendors (e.g. Shear Wave Elastography from SuperSonic Imagine, Virtual Touch^{TM} quantification from Philips/Siemens (5,70)), but these are primarily used for liver and breast tissue and are not optimized yet for cardiac applications. For natural SWE, tissue Doppler imaging (TDI) applications on current clinical scanners can be used. Indeed, Pislaru et al. (71) reported a frame rate of 350-460 Hz on the GE Vivid E9 and Philips iE33 scanner. This can even be elevated to 400-700 Hz on the Philips iE33 system (72). Recently, Canon Medical Systems provides Shear Wave Dispersion Imaging for determining tissue's viscoelastic properties in case of fibrotic liver disease (49). It can be expected that with time, high-end commercial systems and corresponding software can be made ready for cardiac SWE – natural as well as ARF-based – while evidence of the additional clinical information is building up.

Future perspectives

Best practices in cardiac shear wave elastography

As the number of clinical studies on cardiac SWE is growing, the need for consistent data collection and reporting is urgent, and we formulate some recommendations that may improve SWE accuracy and facilitate comparison of SWE results between studies. With the currently available 2D SWE technology, shear waves are typically tracked in the IVS which is located not

too deep nor too shallow for shear wave generation/tracking. The echocardiographic views are limited to PLAX or PSAX for ARF-based SWE, because a quasi-orthogonal relationship between ultrasound beam and cardiac wall is required for inducing transversal wave motion. On the other hand, for natural shear waves, PLAX or AP4C view can be used. It should however be noted that each view tracks a different component of tissue motion and thus potentially a different wave mode (12). Depending on the technological advancements, more echocardiographic views/regions might be possible in the near future.

A variety of SWE-metrics have been reported in literature (illustrated in Table 3 and Table 4). We strongly discourage reporting a shear or Young's modulus through the use of equations (1) and/or (2), since this is associated with stringent assumptions concerning mechanical properties which do not hold for the myocardium (i.e. linear elasticity, isotropy and bulk size). Figure 10 summarizes our recommendations for data reporting in cardiac SWE in clinical practice. Ideally, future research should clearly report the propagation speed of the traveling wave in the time domain together with the main excited frequency. As it is unclear up to now what type of tissue motion (velocity/acceleration) should best be used to determine wave speed, we suggest to report propagation speeds based on both tissue velocity and acceleration to enable comparison between future studies. Furthermore, it is recommended to also report (Figure 10): (i) system-dependent factors which have a non-negligible effect on SWE results but are inherent to the available SWE modality, (ii) technical settings on which operators do have their say and (iii) population characteristics describing mechanical and biological variations. Concerning technical settings, next to echocardiographic view and cardiac region as discussed before, the M-line for wave speed estimation should be positioned in the middle of the cardiac wall parallel to the border (i.e. along the assumed propagation direction). We suggest to repeat this M-line measurement multiple times for multiple SWE acquisitions and to report the median speed together with its interquartile range (19,40). A more advanced material characterization can be obtained from SWE by studying the wave's frequency behavior (dispersion) or multiple echocardiographic views (anisotropy). However, we note that advanced material characterization can be challenging and is often associated with more variable results in low SNR data which can increase the complexity of inter-study comparisons; as such, we recommend including the group SWS measurements as well in these studies. If the resolution of the imaging system is high enough, transmural wave speed variations can also be studied to investigate the myocardial anisotropy, especially in PSAX (see Figure 8). As the wave propagation direction is unknown for natural SWE, 3D imaging will offer additional insights for advancing material characterization.

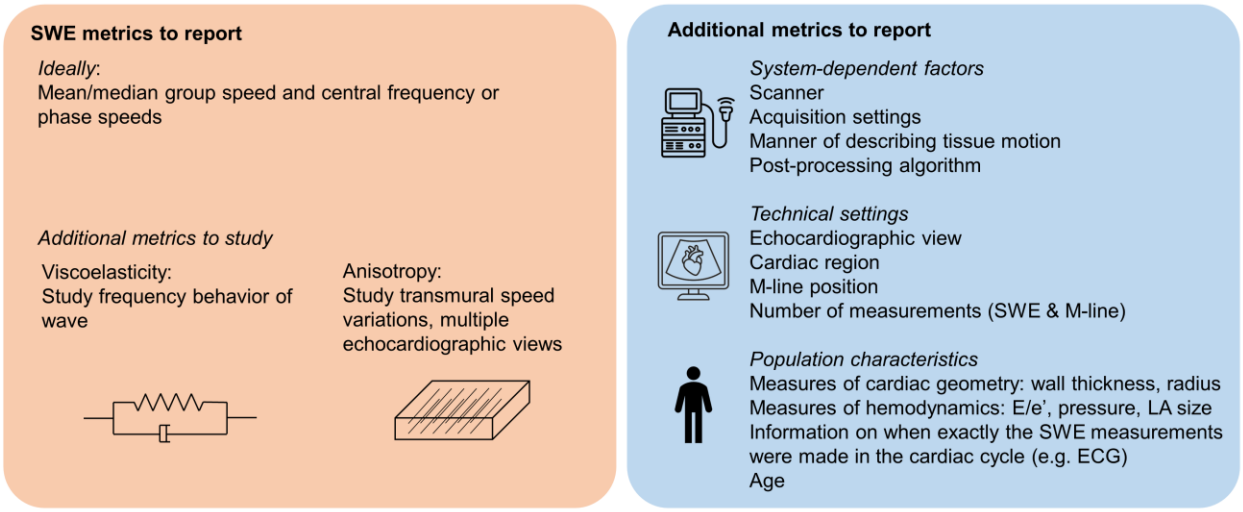

Figure 10 – Recommendations for standardized data reporting based on the currently available SWE technology in the clinics.

Technical and mechanical challenges to overcome

Even though multiple clinical studies have successfully reported results of transthoracic SWE, the technique still faces many challenges of both a technical and mechanical nature. Indeed, the feasibility of transthoracic ARF-based SWE – especially in systole – is generally lower than for natural SWE due to difficulties to transmit a sufficient amount of energy into the cardiac wall for shear wave excitation and to consequently track the generated wave in an acoustically safe manner. This is partly due to location of the heart which is encased by ribs and surrounded by lung tissue limiting the acoustic accessibility. Even though the magnitude of particle motion for natural SWE is higher than for ARF-based SWE (tens of mm/s instead of a few mm/s in Figure 9), the wave speed might be less accurately tracked because of a larger spatial wavelength (a few cm vs. a few mm in Figure 9) within the limited field-of-view (3-4 cm). Additionally, the technical settings of the used elastography mode on the ultrasound scanner (e.g. temporal and spatial characteristics of the ARF, tissue motion estimation algorithm, shear wave speed estimation algorithm, etc.) will also affect the resulting wave speed. A clear communication of the device manufacturer to the sonographers and physicians is necessary to better understand what the system is reporting. We have formulated some guidelines on standardization of SWE data collection and reporting, but it is clear that a dedicated committee endorsed by the leading echography/cardiology societies needs to set these criteria as has been done for the staging of liver fibrosis (Quantitative Imaging Biomarker Alliance by the Radiological Society of North America (67)) and cardiac speckle tracking echocardiography (73).

This paper focused on mechanical factors interfering with cardiac SWE. However, the sensitivity of the SWE technique to each considered mechanical factor remains unclear: is SWE more sensitive to changes in myocardial mechanical properties than to, for example, changes in hemodynamics? And is this different for ARF-based and natural SWE? Furthermore, the arrival of 3D SWE might further improve our understanding of both types of SWE, especially for natural SWE as the spatial and temporal characteristics of the wave excitation source are unknown. It

should also be noted that shear wave measurements provide only a local measurement of stiffness, assessed within the size of the field of view, and it should be further investigated how this relates to global stiffness changes, as reflected by an altered end-diastolic pressure-volume relationship.

Conclusion

Ultrasound-based SWE has a tremendous potential for non-invasive characterization of the active and passive stiffness of the heart. The number of clinical studies demonstrating the discriminative power of shear wave speed for cardiac pathology is growing. However, one should be aware that mechanical factors, next to pathology, affect wave speed estimation. With this paper, we aim to contribute to a better conceptual understanding of shear wave physics and, consequently, a deeper insight for a correct interpretation of findings.

Acknowledgements

This work was supported by the Research Foundation Flanders (FWO, Brussels, Belgium) under grant 1211620N to Annette Caenen.

Kathryn R. Nightingale has intellectual property related to radiation force-based imaging technologies that has been licensed to Siemens, Samsung and MicroElastic Ultrasound Systems. The other authors declare that they have no conflict of interest.

Appendix A: Lamb waves in cardiac SWE

Several studies have used the Lamb wave theory on waves in plates to better understand the geometrical effect on cardiac shear wave propagation (12,24,25,37,74,75). The phase speed characteristics of Lamb waves are displayed in Figure A11a for a representative (isotropic) myocardial model in diastole and systole, in comparison to that of a bulk medium with the same material parameters. While the phase speed characteristics in a bulk medium are independent of frequency (horizontal line; 1.3 m/s in diastole and 4.8 m/s in systole), the phase speeds in a plate increase as a function of frequency until they reach a plateau-value (i.e. the plate wave velocity, which is about 95% of the bulk shear wave velocity (14)). Due to this increasing trend, the group speed is lower than the phase speed. The dispersion curves are defined by the intrinsic features of the cardiac wall (geometry, material model, boundary conditions), and do not depend on any wave excitation properties. It thus dictates the speed with which a frequency component in the generated wave will travel, whereas the bandwidth and central frequency of the excitation will determine which frequencies are excited in the wave. For example, according to the theoretical model displayed in Figure A11a, a traveling mechanical wave with a frequency content between 200-400 Hz in 10 mm thick myocardium will exhibit dispersion when the material is stiffer and more viscous ('Material 2'). On the other hand, a wave with the same frequency content in a 15 mm thick myocardium will not experience any wave dispersion for both materials considered. Low frequency excitations such as natural waves after valve closure are more sensitive to thickness variations: the phase speed can increase 24% (peak frequency of 40 Hz for MVC (18)) in material 1 and 40% in material 2 (peak frequency of 80 Hz for AVC (18)) when myocardial thickness changes from 10 to 15 mm.

Some cardiac SWE studies (24-26,37) have set one step further in post-processing the SWE results by reporting elasticity and viscosity values using the Lamb wave model, as summarized in Table A5. Typically, the cardiac wall is approximated as a fluid-loaded viscoelastic plate, for which a Voigt model is used to describe the rheological behavior. This model assumes a viscous component represented by a dashpot (with viscosity μ_2) in parallel with the elastic component (spring with spring constant μ_1). Both the plate geometry and the viscoelasticity result in a frequency-dependent wave speed. The process to estimate elasticity and viscosity values is as follows. First, the frequency-dependent behavior of the studied mechanical wave is investigated by (i) performing multiple wave speed measurements while varying the frequency of the mechanical actuator (24,25) or by (ii) applying a fast Fourier transform (FFT) on the temporal wave data to analyze the frequency content of the mechanical wave (46,76). Both cases will give the phase speed characteristics as a function of frequency, of which examples are shown for two types of shear wave excitation in Figure A11b. Second, elasticity and viscosity values are obtained by fitting the theoretical Lamb wave model to the measured phase speed characteristics. LV phantom studies (11,77) have shown that the elasticity results based on the phase speed will better approach the true stiffness than those based on the group speed (deviations up to +12% vs. -67%). However, it should be noted that this Lamb wave fitting comes with several assumptions such as plate geometry, smooth walls, and isotropy which do not hold for the cardiac wall. Furthermore, frequency analyses in *in vivo* cardiac SWE are sparsely reported in literature (18,37) because of the non-suitability of mechanical actuators *in vivo* (resulting in a broadband

excitation) and the low resolution in combination with low SNR for an accurate FFT. Furthermore, frequency analysis on natural waves do not allow to get a complete picture of the frequency behavior of the tissue of interest because of their relatively narrow bandwidth <150Hz (18,40).

All reported elasticity and viscosity values in Table A5 are in the same range, except for the systolic elasticity and viscosity reported by Kanai et al. (37) ($\mu_1 = 30\ kPa$ and $\mu_2 = 70 - 400\ Pa \cdot s$), which is larger than the elasticity and viscosity reported by the other studies in Table A5. This might be due to a difference in investigated region (septum vs. free wall), a different view showing different wave types (12) or a variable accuracy in the Lamb wave analysis when the frequency of the wave excitation alters.

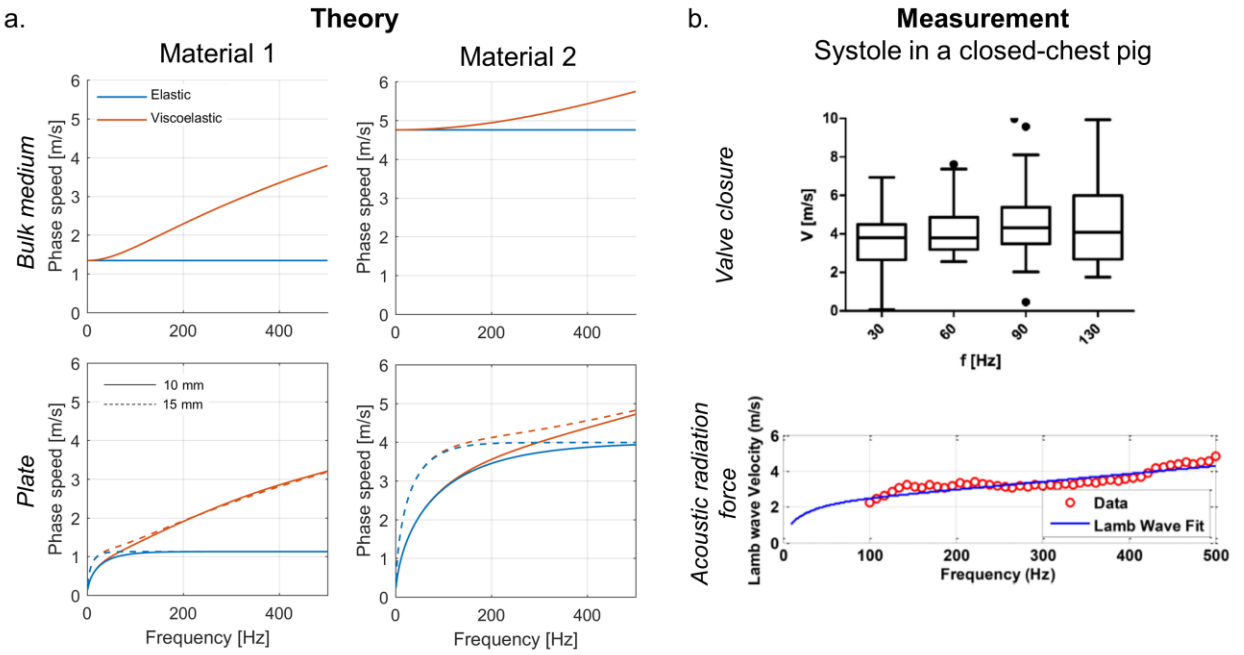

Figure A11 – Effect of geometry and viscoelasticity on shear wave properties. (a) Theoretical predictions of the phase speed variations in a bulk medium and plate (thickness = 10mm), when assuming an elastic and viscoelastic medium (Voigt model). The material parameters are $\mu_1 = 1.8\ kPa$ and $\mu_2 = 2.7\ kPa$ for Material 1; and $\mu_1 = 22.6\ kPa$ and $\mu_2 = 5.9\ kPa$ in Material 2 – as reported by Pislaru et al. (25). Note that the phase speed characteristics of one mode (antisymmetric zero order mode) – expected dominant mode in cardiac SWE – are shown for a fluid-loaded plate. (b) Measured shear wave spectra in a closed-chest pig in systole: group velocities after aortic valve closure (18) (upper panel) and phase velocities in systole after acoustic radiation force application (26) (lower panel). Adapted with permission from Vos et al. (18) and Nenadic et al. (26).

Table A5 – Reported viscoelastic properties in cardiac SWE when assuming a plate-like myocardium with its viscoelastic material properties obeying a Voigt model. Diastolic values in natural SWE corresponds to wave analysis after mitral valve closure; whereas systolic values are obtained for wave analysis after aortic valve closure. (VC: valve closure, MS: mechanical stimulation, ARF: acoustic radiation force, IVS: interventricular septum, LVFW: left ventricular free wall, NR: not reported)

Study (ref #)	Excitation	Region	Species	Diastole		Systole	
				Elasticity μ_1	Viscosity μ_2	Elasticity μ_1	Viscosity μ_2
Kanai et al. (37)	VC	IVS	Human (n=5)	NR	NR	30 kPa	70-400 Pa·s

Urban et al. (24)	MS	LVFW	Open-chest pig (n=8)	1.81±0.8 kPa	2.7±0.56 Pa·s	21.14±7.72 kPa	4.16±4.32 Pa·s
Pislaru et al. (25)	MS	LVFW	Open-chest pig (n=10)	1.8±0.8 kPa	2.7±0.9 Pa·s	22.6±6 kPa	5.9±4.7 Pa·s
Nenadic et al. (26)	ARF	LVFW	Open-chest pig (n=1)	2.24±0.54 kPa	3.36±0.5 Pa·s	12.44±1.3 kPa	3.99±1.19 Pa·s
Nenadic et al. (26)	ARF	LVFW	Pig (n=1)	5.1 kPa	3.2 Pa·s	19.1 kPa	6.8 Pa·s

References

1. Ophir J, Céspedes H, Ponnekanti H, Yazdi Y, Li X. Elastography: A quantitative method for imaging the elasticity of biological tissues. Ultrason Imaging 1991;13:111-134.
2. Gao L, Parker KJ, Lerner RM, Levinson SF. Imaging of the elastic properties of tissue - A review. Ultrasound Med Biol 1996;22:959-977.
3. Villemain O, Baranger J, Friedberg MK et al. Ultrafast Ultrasound Imaging in Pediatric and Adult Cardiology: Techniques, Applications, and Perspectives. JACC Cardiovasc Imaging 2020;13:1771-1791.
4. Ferraioli G, Filice C, Castera L et al. WFUMB guidelines and recommendations for clinical use of ultrasound elastography: Part 3: liver. Ultrasound Med Biol 2015;41:1161-79.
5. Barr RG, Nakashima K, Amy D et al. WFUMB guidelines and recommendations for clinical use of ultrasound elastography: Part 2: breast. Ultrasound Med Biol 2015;41:1148-60.
6. Guimarães CF, Gasperini L, Marques AP, Reis RL. The stiffness of living tissues and its implications for tissue engineering. Nature Reviews Materials 2020;5:351-370.
7. Fung YC. Biomechanics - Mechanical Properties of Living Tissues, 1993.
8. Cobbold RSC. Foundations of Biomedical Ultrasound: Oxford University Press, 2002.
9. Wang M, Byram B, Palmeri M, Rouze N, Nightingale K. Imaging transverse isotropic properties of muscle by monitoring acoustic radiation force induced shear waves using a 2-D matrix ultrasound array. IEEE Trans Med Imaging 2013;32:1671-84.
10. Rouze NC, Wang MH, Palmeri ML, Nightingale KR. Finite element modeling of impulsive excitation and shear wave propagation in an incompressible, transversely isotropic medium. J Biomech 2013;46:2761-8.
11. Caenen A, Pernot M, Shcherbakova DA et al. Investigating Shear Wave Physics in a Generic Pediatric Left Ventricular Model via In Vitro Experiments and Finite Element Simulations. IEEE Trans Ultrason Ferroelectr Freq Control 2017;64:349-361.
12. Keijzer LBH, Strachinaru M, Bowen DJ et al. Parasternal versus Apical View in Cardiac Natural Mechanical Wave Speed Measurements. IEEE Trans Ultrason Ferroelectr Freq Control 2020;67:1590-1602.
13. Greenleaf JF, Fatemi M, Insana M. Selected methods for imaging elastic properties of biological tissues. Annu Rev Biomed Eng 2003;5:57-78.
14. Rose JL. Ultrasonic guided waves in solid media. New York: Cambridge University Press, 2014.
15. Song P, Urban MW, Chen S et al. In vivo tranthoraric measurement of end-diastolic left ventricular stiffness with ultrasound shear wave elastography: a pilot study. IEEE International Ultrasonics Symposium: IEEE, 2014:109-112.
16. Sarvazyan AP, Rudenko OV, Swanson SD, Fowlkes JB, Emelianov SY. Shear Wave Elasticity Imaging: a New Ultrasonics Technology of Medical Diagnostics. Ultrasound Med Biol 1998;24:1419-1435.
17. Nightingale KR, Palmeri ML, Nightingale RW, Trahey GE. On the feasibility of remote palpation using acoustic radiation force. J Acoust Soc Am 2001;110:625-634.
18. Vos HJ, van Dalen BM, Heinonen I et al. Cardiac Shear Wave Velocity Detection in the Porcine Heart. Ultrasound Med Biol 2017;43:753-764.
19. Santos P, Petrescu A, Pedrosa J et al. Natural shear wave imaging in the human heart: normal values, feasibility and reproducibility. IEEE Trans Ultrason Ferroelectr Freq Control 2018;66:442-452.
20. Pislaru C, Pellikka PA, Pislaru SV. Wave propagation of myocardial stretch: correlation with myocardial stiffness. Basic research in cardiology 2014;109:438.

21. Papadacci C, Finel V, Villemain O, Tanter M, Pernot M. 4D Ultrafast Ultrasound Imaging of Naturally Occurring Shear Waves in the Human Heart. IEEE Transactions on Medical Imaging 2020;39:4436-4444.
22. Brekke B, Nilsen LC, Lund J et al. Ultra-high frame rate tissue Doppler imaging. Ultrasound in medicine & biology 2014;40:222-231.
23. Strachinaru M, Geleijnse ML, de Jong N et al. Myocardial Stretch Post-atrial Contraction in Healthy Volunteers and Hypertrophic Cardiomyopathy Patients. Ultrasound Med Biol 2019;45:1987-1998.
24. Urban MW, Pislaru C, Nenadic IZ, Kinnick RR, Greenleaf JF. Measurement of viscoelastic properties of in vivo swine myocardium using lamb wave dispersion ultrasound vibrometry (LDUV). IEEE Trans Med Imaging 2013;32:247-61.
25. Pislaru C, Urban MW, Pislaru SV, Kinnick RR, Greenleaf JF. Viscoelastic properties of normal and infarcted myocardium measured by a multifrequency shear wave method: comparison with pressure-segment length method. Ultrasound Med Biol 2014;40:1785-95.
26. Nenadic IZ, Urban MW, Pislaru C, Escobar D, Vasconcelos L, Greenleaf JF. In Vivo Open- and Closed-chest Measurements of Left-Ventricular Myocardial Viscoelasticity using Lamb wave Dispersion Ultrasound Vibrometry (LDUV): A Feasibility Study. Biomed Phys Eng Express 2018;4.
27. Mariappan YK, Glaser KJ, Ehman RL. Magnetic resonance elastography: a review. Clin Anat 2010;23:497-511.
28. Tzschatzsch H, Elgeti T, Rettig K et al. In Vivo time harmonic elastography of the human heart. Ultrasound Med Biol 2012;38:214-22.
29. Olson TR, Pawlina W. A.D.A.M. Student Atlas of Anatomy, 2008.
30. Hollender PJ, Wolf PD, Goswami R, Trahey GE. Intracardiac echocardiography measurement of dynamic myocardial stiffness with shear wave velocimetry. Ultrasound Med Biol 2012;38:1271-83.
31. Kwiecinski W, Bessiere F, Colas EC et al. Cardiac shear-wave elastography using a transesophageal transducer: application to the mapping of thermal lesions in ultrasound transesophageal cardiac ablation. Phys Med Biol 2015;60:7829-46.
32. Sarvazyan AP, Urban MW, Greenleaf JF. Acoustic Waves in Medical Imaging and Diagnostics. Ultrasound in Medicine & Biology 2013;39:1133-1146.
33. Keijzer LBH, Caenen A, Voorneveld J et al. A direct comparison of natural and acoustic-radiation-force-induced cardiac mechanical waves. Sci Rep 2020;10:18431.
34. Villemain O, Correia M, Mousseaux E et al. Myocardial Stiffness Evaluation Using Noninvasive Shear Wave Imaging in Healthy and Hypertrophic Cardiomyopathic Adults. JACC: Cardiovascular Imaging 2018;12:1135-1145.
35. Couade M, Pernot M, Messas E et al. In vivo quantitative mapping of myocardial stiffening and transmural anisotropy during the cardiac cycle. IEEE Trans Med Imaging 2011;30:295-305.
36. Bouchard R, Hsu D, Wolf P, Trahey G. In Vivo Cardiac Acoustic-Radiation-Force-Driven Shear Wave Velocimetry. Ultrason Imaging 2009;31:201-213.
37. Kanai H. Propagation of spontaneously actuated pulsive vibration in human heart wall and in vivo viscoelasticity estimation. IEEE Trans Ultrason Ferroelectr Freq Control 2005;52:1931-42.
38. Pernot M, Villemain O. In the Heart of Stiffness: Are Natural Heart Vibrations Reliable Enough to Assess Myocardial Stiffness, The New Holy Grail in Echocardiography? JACC Cardiovasc Imaging 2019;12:2399-2401.
39. Salles S, Lovstakken L, Aase SA, Bjastad TG, Torp H. Clutter Filter Wave Imaging. IEEE Trans Ultrason Ferroelectr Freq Control 2019;66:1444-1452.

40. Keijzer LBH, Strachinaru M, Bowen DJ et al. Reproducibility of Natural Shear Wave Elastography Measurements. Ultrasound Med Biol 2019;45:3172-3185.
41. Song P, Zhao H, Urban MW et al. Improved shear wave motion detection using pulse-inversion harmonic imaging with phased array transducer. IEEE Trans Med Imaging 2013;32:2299-2310.
42. Montaldo G, Tanter M, Bercoff J, Benech N, Fink M. Coherent Plane-Wave Compounding for Very High Frame Rate Ultrasonography and Transient Elastography IEEE Trans Ultrason Ferroelectr Freq Control 2009;56:489-506.
43. Kasai C, Namekawa K, Koyano A, Omoto R. Real-Time Two-Dimensional Blood Flow Imaging Using an Autocorrelation Technique. IEEE Trans Sonics Ultrasonics 1985;SU-32:458-464.
44. Pernot M, Lee W-N, Bel A et al. Shear wave imaging of passive diastolic myocardial stiffness: stunned vs infarcted myocardium. JACC Cardiovasc Imaging 2016;9:1023-1030.
45. Parker KJ, Ormachea J, Hah Z. Group versus Phase Velocity of Shear Waves in Soft Tissues. Ultrason Imaging 2018;40:343-356.
46. Deffieux T, Montaldo G, Tanter M, Fink M. Shear wave spectroscopy for in vivo quantification of human soft tissues visco-elasticity. IEEE Trans Med Imaging 2009;28:313-22.
47. Salles S, Espeland T, Molares A et al. 3D Myocardial Mechanical Wave Measurements. JACC: Cardiovascular Imaging 2020.
48. Bercoff J, Tanter M, Muller M, Fink M. The Role of Viscosity in the Impulse Diffraction Field of Elastic Waves Induced by the Acoustic Radiation Force. IEEE Trans Ultrason Ferroelectr Freq Control 2004;51:1523-1536.
49. Sugimoto K, Moriyasu F, Oshiro H et al. Clinical utilization of shear wave dispersion imaging in diffuse liver disease. Ultrasonography 2020;39:3-10.
50. Lee WN, Pernot M, Couade M et al. Mapping myocardial fiber orientation using echocardiography-based shear wave imaging. IEEE Trans Med Imaging 2012;31:554-62.
51. Lee WN, Larrat B, Pernot M, Tanter M. Ultrasound elastic tensor imaging: comparison with MR diffusion tensor imaging in the myocardium. Phys Med Biol 2012;57:5075-95.
52. Caenen A, Pernot M, Peirlinck M, Mertens L, Swillens A, Segers P. An in silico framework to analyze the anisotropic shear wave mechanics in cardiac shear wave elastography. Physics in medicine and biology 2018;63.
53. Bezy S, Cvijic M, Petrescu A et al. Shear wave propagation velocity after aortic valve closure could be a novel parameter for myocardial contractility. European Heart Journal - Cardiovascular Imaging 2020;21.
54. Vejdani-Jahromi M, Freedman J, Nagle M, Kim Y-J, Trahey GE, Wolf PD. Quantifying Myocardial Contractility Changes Using Ultrasound-Based Shear Wave Elastography. J Am Soc Echocardiogr 2017;30:90-96.
55. Pernot M, Couade M, Mateo P, Crozatier B, Fischmeister R, Tanter M. Real-time assessment of myocardial contractility using shear wave imaging. J Am Coll Cardiol 2011;58:65-72.
56. Vejdani-Jahromi M, Freedman J, Kim Y-J, Trahey GE, Wolf PD. Assessment of Diastolic Function Using Ultrasound Elastography. Ultrasound Med Biol 2018;44:551-561.
57. Vejdani-Jahromi M, Nagle M, Jiang Y, Trahey G, Wolf P. A comparison of acoustic radiation force derived indices of cardiac function in the Langendorff perfused rabbit heart. IEEE Trans Ultrason Ferroelectr Freq Control 2016;63:1288-1295.
58. Bezy S, Duchenne J, Orlowska M et al. The behaviour of natural shear waves under different loading conditions. European Heart Journal 2020;41.

59. Hollender P, Bradway D, Wolf P, Goswami R, Trahey G. Intracardiac acoustic radiation force impulse (ARFI) and shear wave imaging in pigs with focal infarctions. IEEE Trans Ultrason Ferroelectr Freq Control 2013;60:1669-82.
60. Keijzer LBH, Bosch JG, Verweij MD, De Jong N, Vos HJ. Intrascan variability of natural shear wave measurements. IEEE International Ultrasound Symposium. Washington DC, USA, 2018:1-4.
61. Vejdani-Jahromi M, Nagle M, Trahey GE, Wolf PD. Ultrasound shear wave elasticity imaging quantifies coronary perfusion pressure effect on cardiac compliance. IEEE Trans Med Imaging 2015;34:465-73.
62. Cvijic M, Bezy S, Petrescu A et al. Interplay of cardiac remodelling and myocardial stiffness in hypertensive heart disease: a shear wave imaging study using high-frame rate echocardiography. Eur Heart J Cardiovasc Imaging 2020;21:664-672.
63. Bezy S, Petrescu A, Cvijic M et al. Determinants of the propagation velocity of natural shear waves in cardiac shear wave elastography. IEEE International Ultrasound Symposium. Las Vegas, NV, USA, 2020.
64. Strachinaru M, Bosch JG, van Gils L et al. Naturally Occurring Shear Waves in Healthy Volunteers and Hypertrophic Cardiomyopathy Patients. Ultrasound Med Biol 2019;45:1977-1986.
65. Petrescu A, Santos P, Orlowska M et al. Velocities of Naturally Occurring Myocardial Shear Waves Increase With Age and in Cardiac Amyloidosis. JACC Cardiovasc Imaging 2019;12:2389-2398.
66. Petrescu A, Bezy S, Cvijic M et al. Shear Wave Elastography Using High-Frame-Rate Imaging in the Follow-Up of Heart Transplantation Recipients. JACC Cardiovasc Imaging 2020;13:2304-2313.
67. Palmeri ML, Milkowski A, Barr R et al. Radiological Society of North America/Quantitative Imaging Biomarker Alliance Shear Wave Speed Bias Quantification in Elastic and Viscoelastic Phantoms. J Ultrasound Med 2021;40:569-581.
68. Trutna CA, Rouze NC, Palmeri ML, Nightingale KR. Measurement of Viscoelastic Material Model Parameters Using Fractional Derivative Group Shear Wave Speeds in Simulation and Phantom Data. IEEE Trans Ultrason Ferroelectr Freq Control 2020;67:286-295.
69. Song P, Bi X, Mellema DC et al. Quantitative Assessment of Left Ventricular Diastolic Stiffness Using Cardiac Shear Wave Elastography: A Pilot Study. J Ultrasound Med 2016;35:1419-27.
70. Sigrist RMS, Liau J, Kaffas AE, Chammas MC, Willmann JK. Ultrasound Elastography: Review of Techniques and Clinical Applications. Theranostics 2017;7:1303-1329.
71. Pislaru C, Alashry MM, Thaden JJ, Pellikka PA, Enriquez-Sarano M, Pislaru SV. Intrinsic Wave Propagation of Myocardial Stretch, A New Tool to Evaluate Myocardial Stiffness: A Pilot Study in Patients with Aortic Stenosis and Mitral Regurgitation. J Am Soc Echocardiogr 2017;30:1070-1080.
72. Strachinaru M, Bosch JG, van Dalen BM et al. Cardiac Shear Wave Elastography Using a Clinical Ultrasound System. Ultrasound Med Biol 2017;43:1596-1606.
73. Voigt JU, Pedrizzetti G, Lysyansky P et al. Definitions for a common standard for 2D speckle tracking echocardiography: consensus document of the EACVI/ASE/Industry Task Force to standardize deformation imaging. Eur Heart J Cardiovasc Imaging 2015;16:1-11.
74. Nguyen T-M, Couade M, Bercoff J, Tanter M. Assessment of Viscous and Elastic Properties of Sub-Wavelength Layered Soft Tissues Using Shear Wave Spectroscopy: Theoretical Framework and In Vitro Experimental Validation. IEEE Trans Ultrason Ferroelectr Freq Control 2011;58:2305-2315.

75. Nenadic IZ, Urban MW, Mitchell SA, Greenleaf JF. Lamb wave dispersion ultrasound vibrometry (LDUV) method for quantifying mechanical properties of viscoelastic solids. Phys Med Biol 2011;56:2245-64.
76. Couade M, Pernot M, Prada C et al. Quantitative assessment of arterial wall biomechanical properties using shear wave imaging. Ultrasound Med Biol 2010;36:1662-76.
77. Sabbadini A, Caenen A, Vos HJ, de Jong N, Verweij MD. Numerical model of Lamb wave propagation in the tapered septal wall of the heart. 2019;39:020003.